Capillarity

Vol. 13, No. 2, p. 37-46, 2024

Original article

Reactive transport modelling of in-situ CO_2 mineralization in basalt formations

Yongqiang Chen[1,2]*, Ben Clennell[1], Junfang Zhang[1], Ming Tang[1,2,3], Shehzad Ahmed[1]

[1]*Energy RU, CSIRO, Kensington WA 6151, Australia*

[2]*Permanent Carbon Locking Future Science Platform, CSIRO, 26 Dick Perry Ave, Kensington WA 6151, Australia*

[3]*School of Energy and Safety, State Key Laboratory of Mining Response and Disaster Prevention and Control in Deep Coal Mines, Anhui University of Science and Technology, Huainan 232001, P. R. China*

Keywords:
In-situ CO_2 mineralization
basalt
reactive transport modelling
permanent carbon removal

Cited as:
Chen, Y., Clennell, B., Zhang, J., Tang, M., Ahmed, S. Reactive transport modelling of in-situ CO_2 mineralization in basalt formations. Capillarity, 2024, 13(2): 37-46.
https://doi.org/10.46690/capi.2024.11.02

Abstract:
In-situ CO_2 mineralization has been identified as a permanent, scalable, large-scale, and potentially cost-effective carbon removal technology. The CO_2 injected into basalt formations can be transformed into carbonate minerals within 2-4 years and thus achieve permanent carbon locking. To understand the *in-situ* CO_2 mineralization, this study aims to fill the knowledge gap in characterizing spatial-temporal geochemical development during *in-situ* CO_2 mineralization. A reactive transport model was thus developed and strictly validated. The model shows an excellent agreement with the standard reactive transport model distributed with PHREEQC. Both the distribution and concentration of aqueous species show an excellent consistency. As indicated by our reactive transport model, $MgCO_3$ is the most carbonate mineral that the cations in the solute can potentially form with a concentration up to 0.26 mol/L while $CaCO_3$ is the second most carbonate mineral, with a maximum concentration of 0.15 mol/L. $FeCO_3$ is the least generated carbonate mineral with a concentration of less than 0.0018 mol/L. Furthermore, our modelling indicates that 48% of carbon is transferred into carbonate minerals while the remaining 52% of carbon exists in aqueous complexes, revealing the importance of dissolution trapping in basaltic formations. Moreover, more carbonate minerals can precipitate in a heterogeneous permeability than an isotropic permeable rock. This study provides insights into the reactive transport process of *in-situ* CO_2 mineralization, which is useful for understanding the underpinning mechanisms and optimizing the petrophysical recipe to maximize the carbon removal potential at the field scale.

1. Introduction

Underground CO_2 storage (UCS) has been identified as an effective way to mitigate the greenhouse effect induced by anthropogenetic gas emissions (Metz et al., 2005). The UCS injects the CO_2 into underground space for sequestrate through four mechanisms (Chen et al., 2023; Zhong et al., 2023), including residual trapping (Pentland et al., 2011; Iglauer et al., 2011; Saeedi et al., 2012), structural trapping (Iglauer et al., 2015), dissolution trapping (Ennis-King and Paterson, 2007), and mineral trapping (Pearce et al., 2022a, 2022b; Turner et al., 2022). As shown in Fig. 1, both structural and residual trapping rely on the capillary force, which immobilizes the CO_2 ganglions in the pore structure. Dissolution trapping refers to CO_2 uptake in saline water. In the above three trapping mechanisms, the CO_2 has the risk of escaping

Yandy Scientific Press

*Corresponding author.
E-mail address: yongqiang.chen@csiro.au (Y. Chen); ben.clennell@csiro.au (B. Clennell); junfang.zhang@csiro.au (J. Zhang); ming.tang@csiro.au (M. Tang); shehzad.ahmed@csiro.au (S. Ahmed).

Received August 10, 2024; revised September 1, 2024; accepted September 21, 2024; available online September 24, 2024.

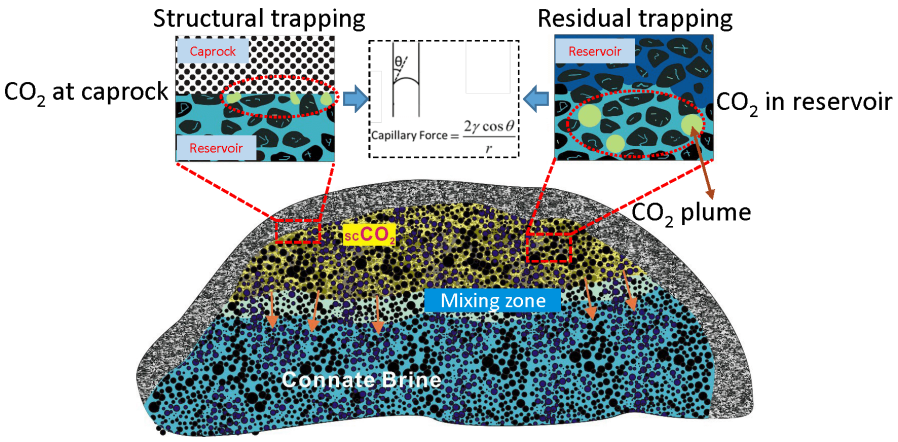

Fig. 1. Schematic graph for structural and residual trapping (Chen et al., 2023).

the trap and leaking to the surface. Mineral trapping transforms the CO_2 into carbonate minerals, such as calcite, magnesite, and dolomite, so is a key trapping mechanism to lock the CO_2 permanently. However, conventional mineral trapping can take thousands of years to achieve (De Silva et al., 2015).

In-situ CO_2 mineralization is a fast, permanent, scalable, and potentially economical carbon removal method (Kelemen and Matter, 2008; NASEM, 2019; Oelkers et al., 2023). To implement the *in-situ* CO_2 mineralization, the CO_2 is injected into the basalt formations, where the CO_2 transforms into minerals within 2-4 years (rather than thousands of years as in the conventional sandstone aquifers) (Kelemen et al., 2020). The basalt rocks contain highly reactive minerals, such as olivine, pyroxene, basaltic glass, etc. These minerals can release cations, such as Ca^{2+}, Mg^{2+} and Fe^{2+}/Fe^{3+}. This leaching process is a natural weathering. The leached cations react with carbonate and bicarbonate to form carbonate minerals. With proper engineering methods, such as injecting acidic CO_2-rich brine, enhanced weathering can be fulfilled to accelerate this leaching process. The leached cations provide ingredients to react with cations for carbonate mineral formation (Chen et al., 2024).

Two pilot field tests demonstrated the feasibility of *in-situ* CO_2 mineralization in basalt reservoirs. The CarbFix project injected CO_2-charged water into a young basalt formation in Iceland (Ragnheidardottir et al., 2011; Snæbjörnsdóttir et al., 2017). $72\pm5\%$ (a total of 165 ± 8.3 t) of injected CO_2 was transformed into calcite (Pogge von Strandmann et al., 2019). By monitoring the Ca isotope in groundwater, more than 90% of injected CO_2 was estimated to be mineralized within 2 years. Furthermore, the techno-economic estimation showed that 90% of the cost stems from CO_2 capturing rather than the *in-situ* CO_2 mineralization itself (Gunnarsson et al., 2018). Carbonated brine injection requires high water usage (about 25 tonnes of water are required to fix every tonne of CO_2 according to Oelkers et al. (2023)), although impacts on water resources could be mitigated by using seawater in coastal locations, or wastewater or recycled water elsewhere.

The Wallula Basalt Pilot Project injected supercritical CO_2 gas into the Columbia River Basalt Group (McGrail et al., 2014), which is a young large flood basalt province mainly formed from ca. 13 to 6 Ma (Camp and Hanan, 2008). In the petrophysical studies and carbon monitoring, McGrail et al. (2017) reported that 1,000 m^3 tons of CO_2 was injected into the targeted field. Vesicles in the cores obtained within the injection zones proved the formation of carbonate minerals ($Ca[Fe, Mg, Mn](CO_3)_2$) in the period 2 years after injection (McGrail et al., 2017). Carbon isotope analysis identified chemically distinct carbonate minerals, which are closely related to injected CO_2 but different from natural carbonate minerals in the basalt (McGrail et al., 2017). These studies demonstrate the feasibility of implementing fast *in-situ* CO_2 mineralization with CO_2 gas. However, compared to the CarbFix project, the efficiency of the Wallula Basalt Pilot Project remains to be assessed.

Reactive transport modelling has been demonstrated as an effective method to unravel the fate of CO_2 for CO_2 storage in subsurface sandstone or carbonate reservoirs. Liu et al. (2019) reviewed current reactive transport algorithms and available codes for UCS. To simulate the flow and reaction, sequential method and global implicit method are implemented. The sequential method calculates the velocity field first, which is then substituted into the transport-reaction equation for reactive transport. The global implicit method calculates the flow, transport, and reaction simultaneously. Most current simulators employ these two algorithms, such as PFLOTRAN (Hammond et al., 2014), TOUGHREACT (Xu et al., 2012), CMG-GEM, OpenGeoSys, PHREEQC (Charlton and Parkhurst, 2011), CrunchFlow (Steefel et al., 2015), HYTEC (van der Lee et al., 2003), ORCHESTRA (Meeussen, 2003), STOMP (White and Oostrom, 2003), MIN3P (Mayer et al., 2002), and NUFT (Hao et al., 2013). These simulators employ various thermodynamic databases to evaluate the CO_2 evolution in various reservoirs. However, few simulations have been performed for *in-situ* CO_2 mineralization in basalt formations. Furthermore, available simulators may be constrained to a specific geological setting. For example, PFLOTRAN, TOUGHREACT, and NUFT select Darcy's law as the flow equation, which only applies to continuum flow while not capable of capturing th-

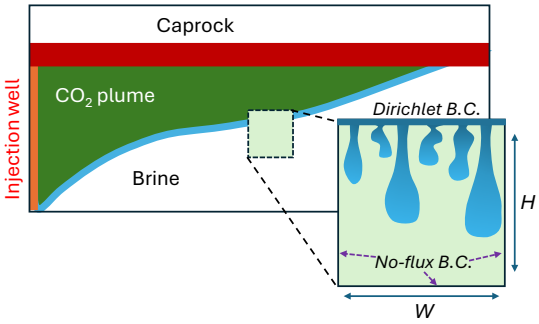

Fig. 2. Schematic graph of the density-driven reactive flow (B.C. is the abbreviation of the boundary condition).

e pore scale flow governed by the Navier-Stokes equation. This drives the development of a reactive transport solver, which couples a general flow solver and geochemical code.

Although the technical feasibility of *in-situ* CO_2 mineralization with carbonated brine injection has been proved, a knowledge gap is a limited understanding of *in-situ* CO_2 mineralization from a dynamic perspective, that is the spatial-temporal development of rock and CO_2-charged water properties. This understanding is required for techno-economic analysis of proposed *in-situ* carbonation projects, to predict and reduce the requirement for water and energy utilization, and to minimise any adverse environmental impacts from the process. Furthermore, CO_2-charged water is denser than plain brine, which drives the downward flow and triggers CO_2 mineralization reactions along the flow path (Fig. 2). Few current studies focus on this issue, which causes uncertainties and a lack of theoretical foundation to optimize the operation strategy of *in-situ* CO_2 mineralization. Variations in ion content and pH of the groundwater also lead to large changes in which minerals precipitate, and where potentially minerals such as clays can precipitate and block reactive surfaces, or carbonates can be deposited too close to the point of CO_2 injection, blocking the injectivity of wells (Wolff-Boenisch and Galeczka, 2018). In general, permeability increases or decreases are found to depend on the flow rates as well as geometries and physical conditions prevailing *in-situ* conditions (Cao et al., 2024). To tackle these challenges, a reactive transport modelling method was thus developed to understand the *in-situ* CO_2 mineralization process that would be applicable across a wide range of pressure, temperature, and compositional scenarios. Briefly, this study aims to fill the knowledge gaps of

1) developing and validating a reactive transport solver for *in-situ* CO_2 mineralization;
2) unravelling the carbonate mineralization process spatially and temporally;
3) comparing the reactive transport modelling with batch modelling.

2. Methodology

2.1 Modelling strategy

A key challenge in reaction transport modelling is preserving realism and details in the geochemistry while making the system tractable for solution in a dynamic flow environment.

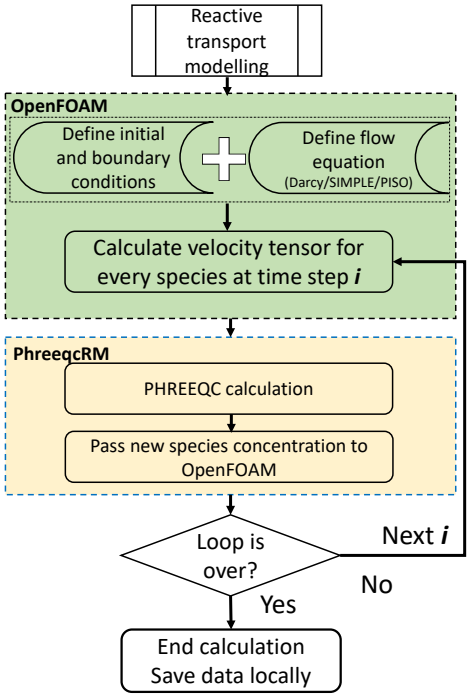

Fig. 3. Schematic graph of reactive transport modelling (operator-splitting method refers to the separate computation of geochemical reaction and flow as shown in the above figure).

Typically, a compromise is made, with restrictions to the geochemical library used, and or simplification of the reactions to a subset of components, species and mechanisms. An existing and well-documented codes was elected to use for the chemical and flow subsystems, and then couple them together. This approach allows changes to the flow subsystem to be made (e.g. to explore pore-scale, continuum scale or field scale situations) but retains the same chemical solver. In this paper, to demonstrate the approach, a reaction transport modelling was looked at the continuum scale (cm to tens of metres in dimension) in a weakly heterogeneous flow field, without the complexities that occur either at the micro scale (i.e., changes to the geometry of individual pores as minerals dissolve or are precipitated), or at the macro scale (i.e., gross geological heterogeneities).

To model the interaction between CO_2-saturated brines and basalt rock, the PHREEQCRM (version 3.7.3-15968) was utilized for geochemical reactions (Parkhurst and Wissmeier, 2015). PHREEQCRM is a reaction module for transport simulators designed from the geochemical code PHREEQC, both of which were written in C++ language. To model the fluid flow, the finite volume method is selected and implemented by leveraging the OpenFOAM (version 2312) library (Weller et al., 1998), which is a well-tested numerical library to solve large scale partial differential equations (PDEs) in parallel. The operator-splitting method (Kanney et al., 2003; Carrayrou et al., 2004) is employed for reactive transport modelling. Fig. 3 is a schematic graph for the coupling process of flow and geochemical reaction.

Table 1. Mineral composition of basalt rocks (Chen et al., 2024).

Mineral composition	Percentage
Olivine (20% fayalite and 80% forsterite)	13
Plagioclase (30% albite and 70% anorthite)	43
Pyroxene (diopside)	39
Basaltic glass	5

Notes: Given the small volume (5%) percentage of basaltic glass, the effect of basaltic glass is not considered in the model.

2.2 Geochemistry setup

The mineral and brine compositions are extracted from Chen et al. (2024). The thermodynamic dataset is from the LLNL database (Lu et al., 2022). The CO_2-saturated brine is injected into the basalt reservoirs to mimic the conditions of the CarbFix project. In this study, the primary species are obtained and to be transported with the C programming language methods in PHREEQCRM. After each reaction step, the secondary species are acquired with the method from PHREEQCRM and output to files. Given the fast reactive character of basalt rocks (Oelkers et al., 2018), the local equilibrium approach was choose in this study (Islam et al., 2016; Babaei and Islam, 2018; Erfani et al., 2021).

The inlet brine is a fully carbonated brine, which is equilibrated at 25 °C, 10 bar. The initial brine in the reservoir is considered a plain brine containing 0.001 mol/L NaCl and equilibrated with basaltic host rock. The host rock contains minerals reported by Aradóttir et al. (2012), in Tables 3 and 4. The mineral composition is briefly listed in Table 1. During the reactive transport flow, the reactions in Table 2 are computed by PHREEQC to evaluate the leaching and precipitation process.

2.3 Flow equation and boundary conditions

In this study, the darcy flow is modelled at a continuum scale. The density-driven flow is modelled in a basalt aquifer. Due to the brine being charged with CO_2, its density increases, which creates a density difference and drives the downward fluid flow. In this study, a density-driven reactive transport model was established to evaluate the geochemical reactions coupled flow in the basalt aquifer.

All the simulations are performed with the following assumptions:

1) The aquifer is assumed to be fully saturated and chemically equilibrated with brine.
2) The fluids are assumed to be incompressible.
3) The temperature is assumed to be constant in the aquifer (applicable where flow rates slow and reactions occur at the interfaces between extensive volumes of fluid and rock).
4) The flow domain is assumed to be a porous continuum instead of discrete pores, vugs or fractures.
5) The porosity and permeability are assumed to not change significantly during the simulation, the same as Islam et al. (2016).
6) All boundaries are assumed to be closed (no flow) except the top boundary, where the CO_2-saturated brine enters the domain.
7) The diffusion coefficients are assumed to be constant and at the level of the water molecular diffusivity, i.e., 1×10^{-9} m^2/s.

The governing equations include the following two parts:

1) Flow and continuity equations of density-driven flow:

$$\boldsymbol{u} = -\frac{K}{\mu}(\nabla p + \rho g \vec{\boldsymbol{n}}_z) \tag{1}$$

$$\nabla \cdot \boldsymbol{u} = 0 \tag{2}$$

where $\boldsymbol{u}$ is flow velocity, m/s; K is permeability, m^2; μ is the viscosity, m^2; ρ is the density, kg/m^3; g is the gravity acceleration, 9.8 m^2/s; $\vec{\boldsymbol{n}}_z$ is a dimensionless unit vector pointing upward.

2) Convection and diffusion equation of reactive species:

$$\frac{\partial c_i}{\partial t} + \boldsymbol{u} \cdot \nabla c_i = \nabla \cdot (\mathbf{D}_i \nabla c_i) + \underbrace{S_i}_{Reactions} \tag{3}$$

where c_i is the concentration of species i, mol/kg; $\mathbf{D}_i$ is the diffusion coefficient of species i; S_i denotes the sink/source term due to the geochemical reaction of species.

2.4 Computation configuration

The domain is a 2-dimensional rectangular with a $10 \times 1 \times 10$ m dimension. The domain is meshed to $100 \times 1 \times 100$ units with the aid of the blockMesh utility provided by the OpenFOAM library. The Laplacian operator in both the momentum and advection-diffusion equation is discretized by the Gauss linearUpwind method (Warming and Beam, 1976). The pressure matrix is solved by the preconditioned conjugate gradient (PCG) algorithm. The preconditioned bi-conjugate gradient (PBiCGStab) algorithm is selected to solve the matrix of each primary species' concentration. All the patches are no flux boundaries except the upper path, which is a Dirichlet boundary, where the CO_2-charged water is assigned. To accurately model the CO_2-charged water at the upper boundary, a boundary condition was code to include the concentrations of all the primary species. The developed model is computed in the Petrichor HPC and visualized in ParaView (version 5.13) (Ahrens et al., 2005).

3. Results and discussion

3.1 Model validation against standard reactive transport model

To validate the developed reactive transport model, the modelling results were compare with the ion exchange model distributed with PHREEQC. Our previous calculation showed

Table 2. Geochemical reactions of *in-situ* CO_2 mineralization (Chen et al., 2024).

Mineral	Reaction	Reaction location/type	log *K*
Albite	$NaAlSi_3O_8 + 4H^+ = Al^{3+} + Na^+ + 2H_2O + 3SiO_2$	Host rock/dissolution	2.7645
Anorthite	$CaAl_2(SiO_4)_2 + 8H^+ = Ca^{2+} + 2Al^{3+} + 2SiO_2 + 4H_2O$	Host rock/dissolution	26.578
Fayalite	$Fe_2SiO_4 + 4H^+ = SiO_2 + 2Fe^{2+} + 2H_2O$	Host rock/dissolution	19.1113
Forsterite	$Mg_2SiO_4 + 4H^+ = SiO_2 + 2H_2O + 2Mg^{2+}$	Host rock/dissolution	27.8626
Diopside	$CaMgSi_2O_6 + 4H^+ = Ca^{2+} + Mg^{2+} + 2H_2O + 2SiO_2$	Host rock/dissolution	20.9643
$CaCO_3$ (Calcite)	$CaCO_3 + H^+ = Ca^{2+} + HCO_3^-$	Aqueous/Mineral precipitation	1.8487
$MgCO_3$ (Magnesite)	$MgCO_3 + H^+ = HCO_3^- + Mg^{2+}$	Aqueous/Mineral precipitation	2.2936
$Mg(OH)_2$ (Brucite)	$Mg(OH)_2 + 2H^+ = Mg^{2+} + 2H_2O$	Aqueous/Mineral precipitation	16.298
$FeCO_3$ (Siderite)	$HCO_3^- + Fe^{2+} = FeCO_3 + H^+$	Aqueous/Mineral precipitation	0.192
Carbonation	$HCO_3^- + H^+ = CO_2 + H_2O$	Aqueous/Carbonation	6.3447

Notes: The thermodynamic data are from Lawrence Livermore National Laboratory thermo.com.V8.R6.230 thermodynamic database.

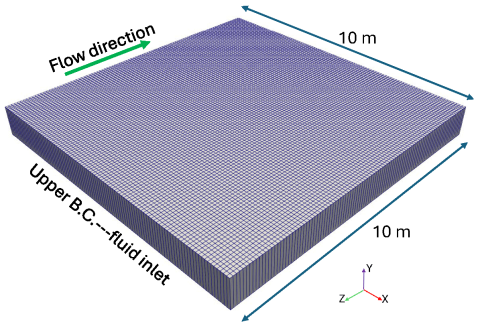

Fig. 4. Configuration and meshing of the computation domain.

that PHREEQC can calculate the ion exchange robust (Chen et al., 2019). In this validation study, the injected brine is set to 0.6 mmol/L $CaCl_2$ while the connate brine contains 1.0 mmol/L Na^+, 0.2 mmol/L K^+, and 1.2 mmol/L NO_3^-. The ion exchange capability is set to be 0.0011 mol/L in all cells. The developed model is a 2-dimensional domain as shown in Fig. 4 while the standard model is a 1-dimensional domain. The concentration data was extracted at a boundary cell adjacent to the outlet patch. The time-dependent data is then transformed to be a function of pore volume (PV) and compared with the concentration-PV data calculated by the PHREEQC. A good agreement is observed between our model and the standard model (as shown in Fig. 5).

Specifically, our model and the standard model show the same trend, switching points, and crossing points. During the $CaCl_2$ injection, the standard model shows a trend that Na^+ drops, K^+ first increases and drops, and both Cl^- and Ca^{2+} increase. Our developed model reflects the same species distribution. Furthermore, the switching points remain consistent between the standard model and the developed model. The switching position for the Cl^- is at 1 PV, the Na^+ is at 1.5 PV, the K^+ is at 1.5 and 2 PV, and the Ca^{2+} is at 2 PV. The new model reflects the same switching configuration. However, the developed model reveals a wider switching zone while the standard model exhibits an abrupt switch. This could be due to the meshing quality and numerical diffusion. The standard model has 40 cells in the domain while the computational domain is discretized into 100 cells for our developed model. Although a slight difference is observed for the switching points, the crossing point between species is the same. For example, the crossing point between the species K^+ and Na^+ is at 0.6 mmol/L while the crossing point between the species K^+ and Ca^{2+} is at 0.4 mmol/L. All three pieces of evidence demonstrate the correctness of the developed model.

3.2 *In-situ* CO_2 mineralization in a basaltic aquifer

The reactive transport model reveals a generation of carbonate minerals during density-driven CO_2-charged brine flow, where the $MgCO_3$ and $CaCO_3$ are the most generated carbonated minerals. Fig. 6 characterizes the distribution of species in the flow domain at Year 0.5, 1, 1.5 and 2.0. $MgCO_3$ is the most abundant carbonate mineral generated in the basaltic formation. Its concentration reaches 0.79 mol/L at the flow front. $CaCO_3$ is the second most generated carbonate mineral. Its highest concentration is around 0.15 mol/L. The amount of $FeCO_3$ is an order of magnitude less than the $MgCO_3$ and $CaCO_3$. This is consistent with the batch modelling from Chen et al. (2024). Both the reactive transport modelling and the batch geochemical modelling demonstrate that magnesite is the most significant product of *in-situ* CO_2 mineralization. However, the reactive transport model indicates that around 0.96 mol/L carbonate minerals are generated out of the total carbonate species of 2 mol/L. Within the domain simulated, 48% of CO_2 becomes mineralized under conditions of local equilibrium, while the other 52% remains in aqueous com-

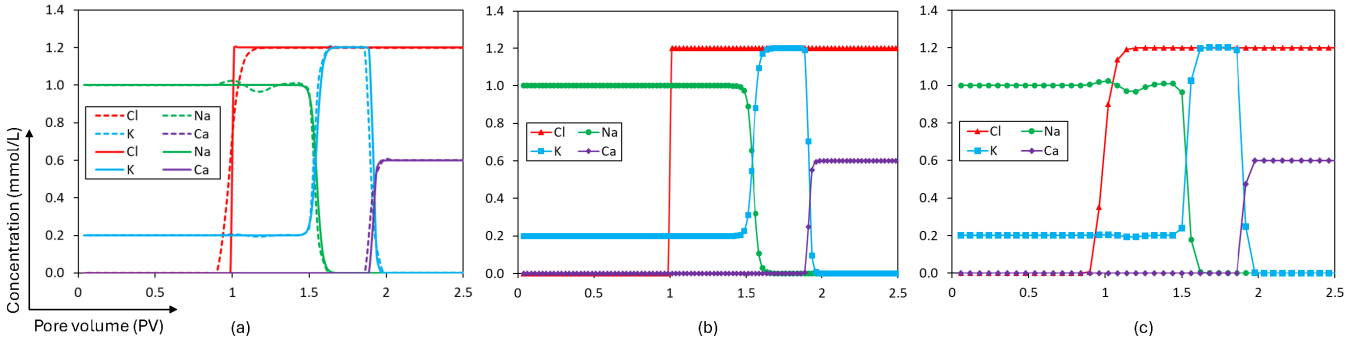

Fig. 5. Modelling results: (a) Solid line is for the standard model. The dash line is for the developed reactive transport model, (b) standard model and (c) developed model.

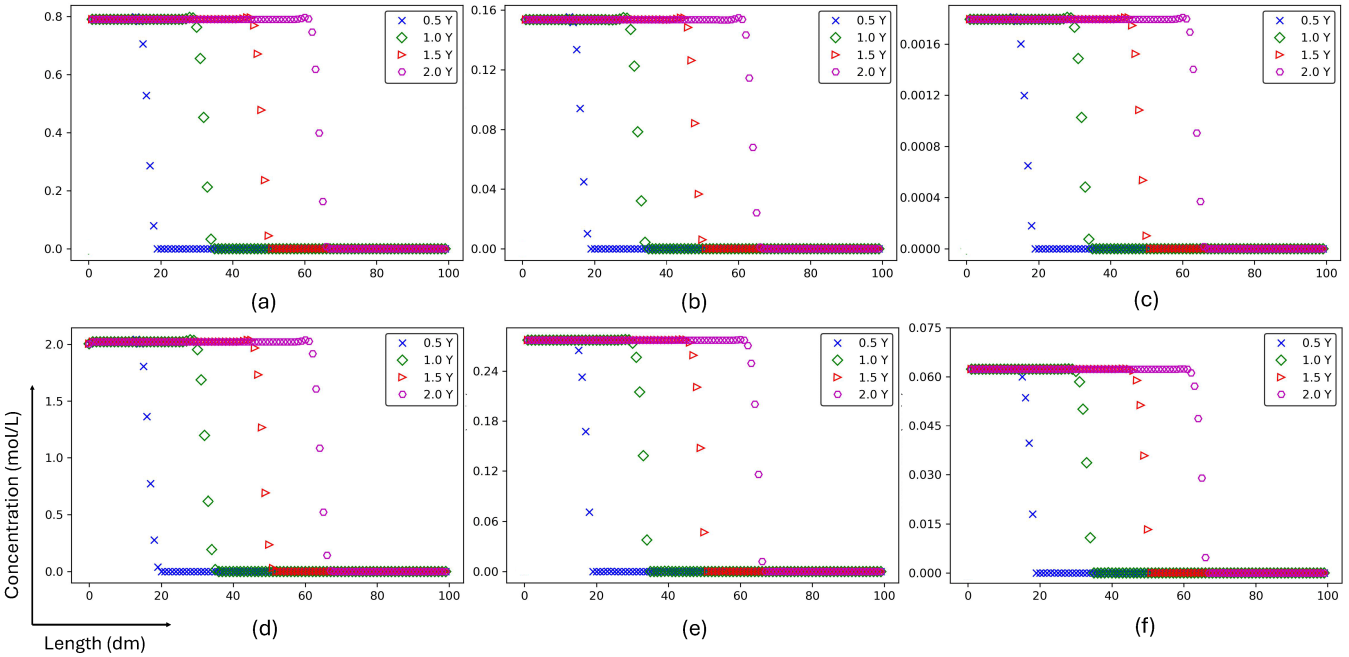

Fig. 6. The concentration of carbonate species at Year 0.5, 1.0, 1.5 and 2.0. (a) $MgCO_3$, (b) $CaCO_3$, (c) $FeCO_3$, (d) total carbon, (e) CO_3^{2-} and (f) HCO_3^-. All species concentration is in a random permeability field as shown in Fig. 7.

plexes and is discharged from the downstream end of the simulation box during continuous flow.

Reactive transport modelling demonstrates that more carbonate minerals are generated during dynamic flow than in a static batch condition. The batch modelling from Chen et al. (2024) shows that the magnesite production increases from nearly 0 to 0.128 mol/L when the system pressure increases from 0.01 to 826.4 psi. The reactive transport modelling reveals that the amount of magnesite can reach 0.79 mol/L. Furthermore, more $FeCO_3$ is generated than $CaCO_3$ in batch modelling. However, the reactive transport modelling proves that more $CaCO_3$ is produced than $FeCO_3$ under flow-through conditions. This study unravels the unique geochemical characteristics of *in-situ* CO_2 mineralization during reactive transport.

In addition, Figs. 7 and 8 show the spatial distribution of carbonate species in a heterogeneous and isotropic flow domain, respectively. In Fig. 8, a sharp front was observed for $MgCO_3$ while a diffusive front is observed for $CaCO_3$ and $FeCO_3$. This could be the stronger reaction between Mg^{2+} and CO_3^{2-} than Ca^{2+} and Fe^{2+}. According to the thermodynamic database, the $\log K$ of $MgCO_3 + H^+ = HCO_3^- + Mg^{2+}$ is 2.29, larger than the $\log K$ of the same reactions of Ca^{2+} and Fe^{2+}, which are 1.85 and 0.19, respectively. So rates of reaction would be 2.7 and 120 times greater for magnesium carbonate than for calcite and for siderite, respectively. Moreover, it reveals that the $MgCO_3$ concentration is dependent on permeability distribution. The peak concentration of $MaCO_3$ reaches 0.79 mol/L in a heterogeneous domain while the peak concentration only reaches 0.26 mol/L in an isotropic permeability field (as demonstrated by the concentration legend of Figs. 7 and 8).

4. Conclusion and implications

In-situ CO_2 mineralization has been identified as a high potential method to offset anthropogenic greenhouse gas emis-

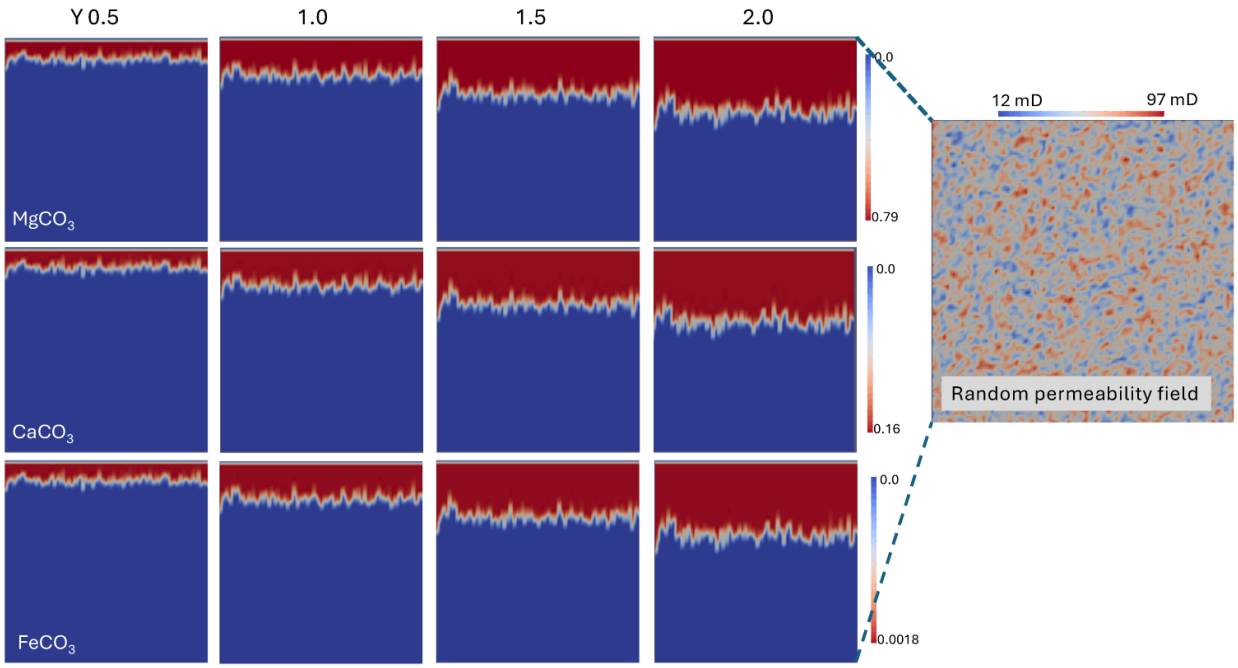

Fig. 7. Distribution of carbonate minerals at Year 0.5, 1.0, 1.5 and 2.0.

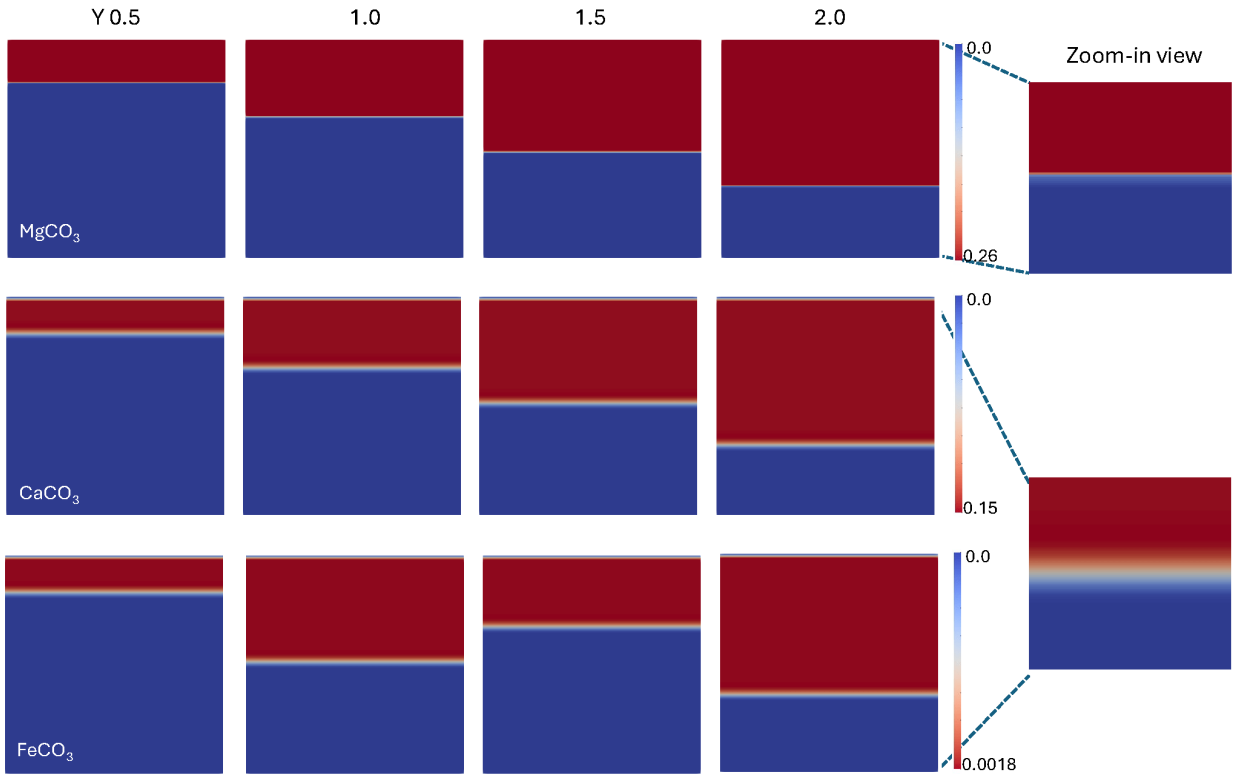

Fig. 8. Distribution of carbonate minerals at Year 0.5, 1.0, 1.5 and 2.0 in an isotropic permeability field (permeability is 150 mD, the right figure is a zoomed-in view of the reactive transport front).

sions. As indicated by the CarbFix and Wallula pilot project, the injected CO_2 is transformed into carbonate rocks within 2 to 4 years, which is a permanent, scalable, fast, and potentially cost-effective carbon removal method. To evaluate the *in-situ* CO_2 mineralization at the continuum scale, a reactive transport model was established by coupling the robust geochemical solver PHREEQC and fluid dynamics engine OpenFOAM.

The new reactive transport model has been validated against the standard model provided by PHREEQC. Both the standard model and the developed model reveal the same trend, switching points, and crossing points of chemical species. The same trend demonstrates that our developed model can precisely predict the trend of geochemical evolution during flow and transport. The same switching and crossing points prove that our developed model can accurately characterize the geochemical reactions between species.

The reactive transport modelling reveals that more CO_2 is transformed into carbonate minerals during reactive transport than batch equilibrium status. Around half of injected CO_2 is mineralized while the other 52% of CO_2 exists as aqueous complexes. The reactive transport modelling further confirms that the dominant precipitated carbonate mineral is magnesite while calcite is the second most abundant carbonate mineral product of the reaction with basalt.

The spatial distribution of carbonate shows a sharp front for $MgCO_3$ while a diffusive front is observed for $CaCO_3$ and $FeCO_3$. This could be due to the high reactive capacity of Mg^{2+} over Ca^{2+} and Fe^{2+}. The reactive transport model unravels that the mineralized carbon is dependent on permeability distribution. In a heterogeneous geological domain, the peak $MgCO_3$ concentration reaches 0.79 mol/L while only 0.26 mol/L $MgCO_3$ is generated in a homogeneous permeable rock.

This study provides insights into the mineral distribution from a dynamic perspective of *in-situ* CO_2 mineralization in basalt formations. However, this study is limited to a simplified geological domain in order to test the robustness of the model. Oelkers et al. (2023) recommends that future research to move *in-situ* carbon mineralization forward focusing on pilot-scale field trials backed up by modelling to investigate and quantify key uncertainties. Lu et al. (2024) recently reviewed experimental work on carbon mineralization in basalt and identified key uncertainties and knowledge gaps. Future experiments need to collect more detailed quantitative information on fluid and mineral compositions and volumes including tracking of the sources and sinks for trace elements as well as major elements to remove ambiguities. Experiments that are co-designed with numerical models ensure that both can honour the complexity of the real-world system.

Our approach is a step towards more accurate modelling of reaction transport across scales from pore and sample scales to field scale processes that can help bridge these gaps. In future studies, greater geological complexity can be included in the model and instabilities can be explored. The code can include perturbations to the inlet boundary to evaluate the effect of compositional-density fingering on the *in-situ* CO_2 mineralization. The heterogeneity of permeability and mineralogy gathered from field observations can be incorporated into the model to further quantify the *in-situ* CO_2 mineralization under real-world reservoir conditions.

Acknowledgements

This study was funded by the Permanent Carbon Locking Future Science Platform, CSIRO under OD-233488. Impossible without you (IWY) project is acknowledged for supporting Yongqiang Chen under OD-233197. Computational resources and expertise are provided by CSIRO IMT Scientific Computing. We thank the constructive communication with David Parkhurst (one of the main developers of PHREEQC).

Conflict of interest

The authors declare no competing interest.

References

Ahrens, J., Geveci, B., Law, C. Paraview: An end-user tool for large-data visualization, in Visualization Handbook, edited by C. D. Hansen and C. R. Johnson, Butterworth-Heinemann, Burlington, pp. 717-731, 2005.

Aradóttir, E. S. P., Sonnenthal, E. L., Björnsson, G., et al. Multidimensional reactive transport modeling of CO_2 mineral sequestration in basalts at the hellisheidi geothermal field, Iceland. International Journal of Greenhouse Gas Control, 2012, 9: 24-40.

Babaei, M., Islam, A. Convective-reactive CO_2 dissolution in aquifers with mass transfer with immobile water. Water Resources Research, 2018, 54(11): 9585-9604.

Camp, V. E., Hanan, B. B. A plume-triggered delamination origin for the columbia river basalt group. Geosphere, 2008, 4(3): 480-495.

Cao, X., Li, Q., Xu, L., et al. A review of in situ carbon mineralization in basalt. Journal of Rock Mechanics and Geotechnical Engineering, 2024, 16(4): 1467-1485.

Carrayrou, J., Mosé, R., Behra, P. Operator-splitting procedures for reactive transport and comparison of mass balance errors. Journal of Contaminant Hydrology, 2004, 68(3): 239-268.

Charlton, S. R., Parkhurst, D. L. Modules based on the geochemical model phreeqc for use in scripting and programming languages. Computers & Geosciences, 2011, 37(10): 1653-1663.

Chen, Y., Saeedi, A., Xie, Q. Interfacial interactions of CO_2-brine-rock system in saline aquifers for CO_2 geological storage: A critical review. International Journal of Coal Geology, 2023, 274: 104272.

Chen, Y., Seyyedi, M., Clennell, B. Petrophysical recipe for *in-situ* CO_2 mineralization in basalt rocks. Advances in Geo-Energy Research, 2024, 11(2): 152-160.

Chen, Y., Xie, Q., Saeedi, A. Role of ion exchange, surface complexation, and albite dissolution in low salinity water flooding in sandstone. Journal of Petroleum Science and Engineering, 2019, 176: 126-131.

De Silva, G. P. D., Ranjith, P. G., Perera, M. S. A. Geochemical aspects of CO_2 sequestration in deep saline aquifers: A review. Fuel, 2015, 155: 128-143.

Ennis-King, J., Paterson, L. Coupling of geochemical reactions and convective mixing in the long-term geological storage of carbon dioxide. International Journal of Greenhouse Gas Control, 2007, 1(1): 86-93.

Erfani, H., Babaei, M., Niasar, V. Dynamics of CO_2 density-driven flow in carbonate aquifers: Effects of dispersion and geochemistry. Water Resources Research, 2021, 57(4): e2020WR027829.

Gunnarsson, I., Aradóttir, E. S., Oelkers, E. H., et al. The rapid and cost-effective capture and subsurface mineral storage of carbon and sulfur at the carbfix2 site. International Journal of Greenhouse Gas Control, 2018, 79: 117-126.

Hammond, G. E., Lichtner, P. C., Mills, R. T. Evaluating the performance of parallel subsurface simulators: An illustrative example with pflotran. Water Resources Research, 2014, 50(1): 208-228.

Hao, Y., Smith, M., Sholokhova, Y., et al. CO_2-induced dissolution of low permeability carbonates. Part II: Numerical modeling of experiments. Advances in Water Resources, 2013, 62: 388-408.

Iglauer, S., Al-Yaseri, A. Z., Rezaee, R., et al. CO_2 wettability of caprocks: Implications for structural storage capacity and containment security. Geophysical Research Letters, 2015, 42(21): 9279-9284.

Iglauer, S., Paluszny, A., Pentland, C. H., et al. Residual CO_2 imaged with X-ray micro-tomography. Geophysical Research Letters, 2011, 38(21): L21403.

Islam, A., Sun, A. Y., Yang, C. Reactive transport modeling of the enhancement of density-driven CO_2 convective mixing in carbonate aquifers and its potential implication on geological carbon sequestration. Scientific Reports, 2016, 6(1): 24768.

Kanney, J. F., Miller, C. T., Kelley, C. T. Convergence of iterative split-operator approaches for approximating nonlinear reactive transport problems. Advances in Water Resources, 2003, 26(3): 247-261.

Kelemen, P. B., Matter, J. In situ carbonation of peridotite for CO_2 storage. Proceedings of the National Academy of Sciences of the United States of America, 2008, 105(45): 17295-17300.

Kelemen, P. B., McQueen, N., Wilcox, J., et al. Engineered carbon mineralization in ultramafic rocks for CO_2 removal from air: Review and new insights. Chemical Geology, 2020, 550: 119628.

Liu, P., Zhang, T., Sun, S. A tutorial review of reactive transport modeling and risk assessment for geologic CO_2 sequestration. Computers & Geosciences, 2019, 127: 1-11.

Lu, P., Apps, J., Zhang, G., et al. Knowledge gaps and research needs for modeling CO_2 mineralization in the basalt-CO_2-water system: A review of laboratory experiments. Earth-Science Reviews, 2024, 254: 104813.

Lu, P., Zhang, G., Apps, J., et al. Comparison of thermodynamic data files for phreeqc. Earth-Science Reviews, 2022, 225: 103888.

Mayer, K. U., Frind, E. O., Blowes, D. W. Multicomponent reactive transport modeling in variably saturated porous media using a generalized formulation for kinetically controlled reactions. Water Resources Research, 2002, 38(9): 13-1-13-21.

McGrail, B. P., Schaef, H. T., Spane, F. A., et al. Field validation of supercritical CO_2 reactivity with basalts. Environmental Science & Technology Letters, 2017, 4(1): 6-10.

McGrail, B. P., Spane, F. A., Amonette, J. E., et al. Injection and monitoring at the wallula basalt pilot project. Energy Procedia, 2014, 63: 2939-2948.

Meeussen, J. C. Orchestra: An object-oriented framework for implementing chemical equilibrium models. Environmental Science Technology, 2003, 37(6): 1175-1182.

Metz, B, Davidson, O., de Coninck, H., et al. Carbon dioxide capture and storage. Cambridge, Cambridge University Press, 2005.

National Academies of Sciences, Engineering, and Medicine (NASEM). Negative emissions technologies and reliable sequestration: A research agenda. Washington, The National Academies Press, 2019.

Oelkers, E. H., Declercq, J., Saldi, G. D., et al. Olivine dissolution rates: A critical review. Chemical Geology, 2018, 500: 1-19.

Oelkers, E. H., Gislason, S. R., Kelemen, P. B. Moving subsurface carbon mineral storage forward. Carbon Capture Science & Technology, 2023, 6: 100098.

Parkhurst, D. L., Wissmeier, L. Phreeqcrm: A reaction module for transport simulators based on the geochemical model phreeqc. Advances in Water Resources, 2015, 83: 176-189.

Pearce, J. K., Brink, F., Dawson, G. W., et al. Core characterisation and predicted CO_2 reactivity of sandstones and mudstones from an australian oil field. International Journal of Coal Geology, 2022a, 250: 103911.

Pearce, J. K., Dawson, G. W., Golding, S. D., et al. Predicted CO_2 water rock reactions in naturally altered CO_2 storage reservoir sandstones, with interbedded cemented and coaly mudstone seals. International Journal of Coal Geology, 2022b, 253: 103966.

Pentland, C. H., El-Maghraby, R., Iglauer, S., et al. Measurements of the capillary trapping of super-critical carbon dioxide in berea sandstone. Geophysical Research Letters, 2011, 38(6): L06401.

Pogge von Strandmann, P. A. E., Burton, K. W., Snæbjörnsdóttir, S. O., et al. Rapid CO_2 mineralisation into calcite at the carbfix storage site quantified using calcium isotopes. Nature Communications, 2019, 10(1): 1983.

Ragnheidardottir, E., Sigurdardottir, H., Kristjansdottir, H., et al. Opportunities and challenges for carbfix: An evaluation of capacities and costs for the pilot scale mineralization sequestration project at hellisheidi, iceland and beyond. International Journal of Greenhouse Gas Control, 2011, 5(4): 1065-1072.

Saeedi, A., Rezaee, R., Evans, B. Experimental study of the effect of variation in *in-situ* stress on capillary residual trapping during CO_2 geo-sequestration in sandstone

reservoirs. Geofluids, 2012, 12(3): 228-235.

Snæbjörnsdóttir, S. Ó., Oelkers, E. H., Mesfin, K., et al. The chemistry and saturation states of subsurface fluids during the in situ mineralisation of CO_2 and H_2S at the carbfix site in sw-iceland. International Journal of Greenhouse Gas Control, 2017, 58: 87-102.

Steefel, C. I., Appelo, C. A. J., Arora, B., et al. Reactive transport codes for subsurface environmental simulation. Computational Geosciences, 2015, 19(3): 445-478.

Turner, L. G., Dawson, G. K. W., Golding, S. D., et al. CO_2 and nox reactions with CO_2 storage reservoir core: Nox dissolution products and mineral reactions. International Journal of Greenhouse Gas Control, 2022, 120: 103750.

van der Lee, J., De Windt, L., Lagneau, V., et al. Module-oriented modeling of reactive transport with hytec. Computers & Geosciences, 2003, 29(3): 265-275.

Warming, R. F., Beam, R. M. Upwind second-order difference schemes and applications in aerodynamic flows. AIAA Journal, 1976, 14(9): 1241-1249.

Weller, H. G., Tabor, G., Jasak, H., et al. A tensorial approach to computational continuum mechanics using object-oriented techniques. Computer in Physics, 1998, 12(6): 620-631.

White, M. D., Oostrom, M. Stomp subsurface transport over multiple phases version 3.0 user's guide. 2003-06-20.

Wolff-Boenisch, D., Galeczka, I. M. Flow-through reactor experiments on basalt-(sea)water-CO_2 reactions at 90 °C and neutral ph. What happens to the basalt pore space under post-injection conditions? International Journal of Greenhouse Gas Control, 2018, 68: 176-190.

Xu, T., Spycher, N., Sonnenthal, E., et al. Toughreact user's guide: A simulation program for non-isothermal multi-phase reactive transport in variably saturated geologic media, version 2.0. Earth Sciences Division, Lawrence Berkeley National Laboratory, Berkeley, USA, 2012.

Zhong, Z., Chen, Y., Fu, M., et al. Role of CO_2 geological storage in china's pledge to carbon peak by 2030 and carbon neutrality by 2060. Energy, 2023, 272: 127165.